COAXIAL MAGNETRON LAUNCHER FOR 2.45 GHZ ISM BAND

V. Bilik

Faculty of Electrical Engineering and Information Technology, Slovak University of Technology, Ilkovicova 3, 81219 Bratislava, Slovak Republic
vladimir.bilik@s-team.sk

Keywords: *microwave industrial applications, microwave components, magnetron launcher, S-parameters.*

Introduction

The emergence in recent years of high-power solid-state microwave generators has resulted in increased interest in applicators with coaxial inputs. Such applicators can also be fed from a cheaper alternative – the magnetron. Traditionally, magnetrons are coupled to rectangular waveguides using *waveguide launchers*. Magnetron Rieke diagrams published in the datasheets are with respect to a specific *reference launcher*, the dimensions of which are provided in the datasheets. A generally accepted reference launcher for low-power 2.45 GHz magnetrons has been standardized by the EIAJ.

To feed a *coaxial* applicator using a waveguide launcher, an additional waveguide-to-coaxial adapter is needed, making the whole system clumsy and unnecessarily bulky. An alternative is a *coaxial launcher* (CL), where the magnetron is coupled directly to a coaxial line. It is particularly appealing because the magnetron antenna is inherently a coaxial structure.

In this paper, we present the design procedure and experimental results (Rieke diagram) of a noncontacting CL with 7/8" EIA coaxial output, appropriate for a class of 2.45-GHz magnetrons with powers up to about 1.5 kW. We have designed the CL for the Panasonic 2M244 magnetron, a good representative of this class. We carried out the design using electromagnetic simulation.

Magnetron Launcher

A magnetron launcher is a microwave component used to establish an optimal coupling between the magnetron's internal resonator system and an external load. There are two conflicting design criteria: (a) for a matched external load, a highest possible magnetron efficiency should be attained; and (b) for mismatched loads with varying phase, the variation of the generated frequency (frequency pulling) should be as small as possible. The first requirement generally calls for a strong coupling, i.e., a heavily loaded internal resonator, while the second requirement demands a weak coupling [1, 2]. A reasonable compromise has been established by magnetron developers when designing waveguide reference launchers (RL), to which magnetron performance charts and Rieke diagrams are related. While designing a launcher from scratch would be practically impossible for an application engineer, a more feasible method is to ensure that a magnetron installed in a new launcher behaves the same as when installed in an existing RL. This is the basic idea behind the design of our CL.

Extended Launcher

Because magnetron antennas physically intrude into launchers, the launchers cannot be treated *per se* but only in conjunction with at least an antenna portion of the magnetrons. We will refer to such a conjunction as to an *extended launcher*. Electrically, an extended launcher is a linear two-port network that transforms a conveniently defined and

measurable external load reflection coefficient Γ_R at an output port 2 to a suitably chosen magnetron *internal* reflection coefficient Γ_x at an input port 1. As shown in Fig. 1, we found such a suitable Γ_x for the 2M244 magnetron. The antenna structure includes a 10-mm long section of a 2 mm/9 mm coaxial line with characteristic impedance Z_{01} = 90.2 Ω. The short choke in the outer conductor plays no role at 2.45 GHz.

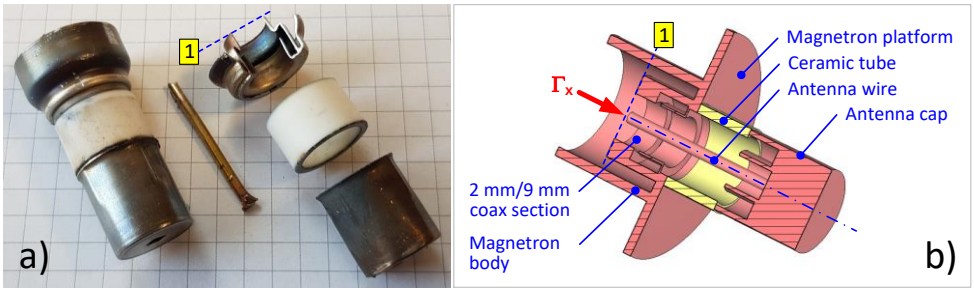

Fig. 1. (a) Antenna of 2M244 magnetron; (b) antenna model with definition of internal reflection coefficient Γ_x and location of port 1 reference plane.

The transform between Γ_R and Γ_x is governed by the network scattering matrix $\boldsymbol{S}$, which now can be readily defined. The input reflection coefficient is

$$\Gamma_x = S_{11} + \frac{S_{12}S_{21}\Gamma_R}{1 - S_{22}\Gamma_R} \qquad (1)$$

A magnetron will have identical behavior in two different launchers if it perceives the same reflection coefficient Γ_x for numerically the same, albeit differently defined load reflection coefficients Γ_R.

Since extended launchers are reciprocal and practically loss-free, their S-parameters are constrained by the relations

$$S_{11} = r\,e^{j\varphi_{11}}, \qquad S_{22} = r\,e^{j\varphi_{22}}, \qquad S_{21} = \sqrt{1-r^2}\,e^{j\varphi_{21}} \qquad (2)$$

$$\varphi_{21} = \frac{\varphi_{11} + \varphi_{22}}{2} - \frac{\pi}{2} + n\pi, \quad n = 0, \pm 1, \pm 2 \ldots \qquad (3)$$

Only three of these quantities are independent: r, φ_{11}, and φ_{22} (the multiplier n is determined by the overall launcher length). The output phase φ_{22} is of little relevance because it only affects the rotation of the Rieke diagram as a whole. Consequently, for design purposes, the launcher is sufficiently described by its S_{11} parameter. The design of a CL reduces to ensuring that S_{11} of the extended coaxial launcher (ECL) is as close as possible to that of the extended reference launcher (ERL). Formally, the task is to minimize in the magnetron tuning range the maximal absolute value of the error vector

$$e_{11}(f) = S_{11}(f) - S_{R11}(f) \qquad (4)$$

where $S_{11}(f)$ refers to ECL and $S_{R11}(f)$ refers to ERL. The target frequency dependence $S_{R11}(f)$ must be known in advance.

Extended Reference Launcher

Fig. 2a shows schematically an extended reference launcher based on the 2M244 antenna structure according to Fig. 1 and the magnetron datasheet [3]. The Γ_R definition plane (port 2) is located at the magnetron antenna axis. The launcher itself is characterized by three main parameters: the waveguide inner dimensions a_r (not shown in Fig. 2a) and b_r, and the distance d_s of the antenna axis from the short-circuited waveguide end. For a wide class of

low-power 2.45-GHz magnetrons these dimensions are a_r = 95.3 mm, b_r = 54.6 mm, d_s = 18.6 mm.

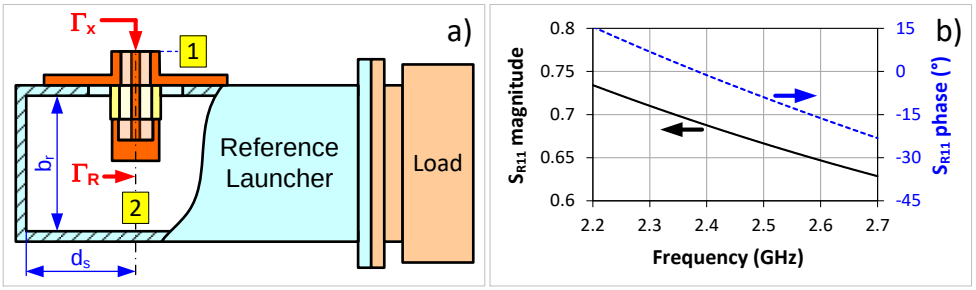

Fig. 2. Extended reference launcher (a) and its S_{R11} (b).

The ERL structure is simple enough to be well amenable to electromagnetic simulation. As our simulation tool, we have used the Dassault Systems CST Studio Suite [4] throughout. There was an uncertainty about the antenna ceramic material, which could be either beryllium oxide BeO ($\varepsilon_r \approx 6$) or alumina Al_2O_3 ($\varepsilon_r \approx 10$). Our own measurements were inconclusive, leading to $\varepsilon_r = 8.1$. Fortunately, the effect of ε_r was found to be insignificant. As a compromise, we used $\varepsilon_r = 8$ in all of our simulations.

The frequency response $S_{R11}(f)$ in the range 2.2 – 2.7 GHz is shown in Fig. 2b. Using a range wider than necessary is good for detecting potential irregularities close to the operating band. At 2.45 GHz, $S_{R11} = 0.68 \angle -5.2°$. We stored the tabulated $S_{R11}(f)$ dependence into a Touchstone-format file. This file later served as the target for optimizing the coaxial launcher.

Because the same reference launcher is specified for many magnetron models, a coaxial launcher designed for one magnetron type (in our case 2M244) will be applicable to a whole class of magnetrons.

Launcher Design Procedure

The basic procedure for designing a coaxial launcher (and, in fact, of any other launcher) can be summarized as follows:

1. Devise a prospective CL internal structure that can potentially meet electrical as well as mechanical criteria (some of which are listed in the next section).
2. Create an electromagnetic simulation model of the *extended* CL.
3. By varying the CL structure dimensions, verify the feasibility of the model by comparing the simulated $S_{11}(f)$ of the ECL with the target $S_{R11}(f)$ of the ERL. Select the two or three variables that are most suitable for optimization. Try to come up with an initial guess of these parameters.
4. Run an optimization routine that minimizes the magnitude of the error function (4) in an appropriate frequency range (e.g., an ISM band). Round off the found optimal dimensions to 0.1 mm for the sake of manufacturability.
5. Thoroughly analyze the final structure for possible weak points (e.g., arcing or local overheating, excessive sensitivity to certain dimensions and material parameters).
6. Build a CL prototype. Measure the Rieke diagram of a 2M244 magnetron installed in the prototype. Repeat the same for the magnetron installed in a reference launcher. Assess the success of the CL design by comparing the two obtained Rieke diagrams.

Designed Coaxial Launcher

The CST model of the designed extended coaxial launcher ECL is shown in Fig. 3. The output is a standard 50-Ω 7/8" EIA coaxial transmission line (with inner and outer diameters 8.7 mm and 20 mm, respectively). We chose this type of the transmission line

because of its robustness and sufficient power rating, which is 1.5 kW at 2.45 GHz. The most natural reference plane (port 2), to which the load reflection coefficient Γ_R as well as the Rieke diagram will be related, is the launcher output flange.

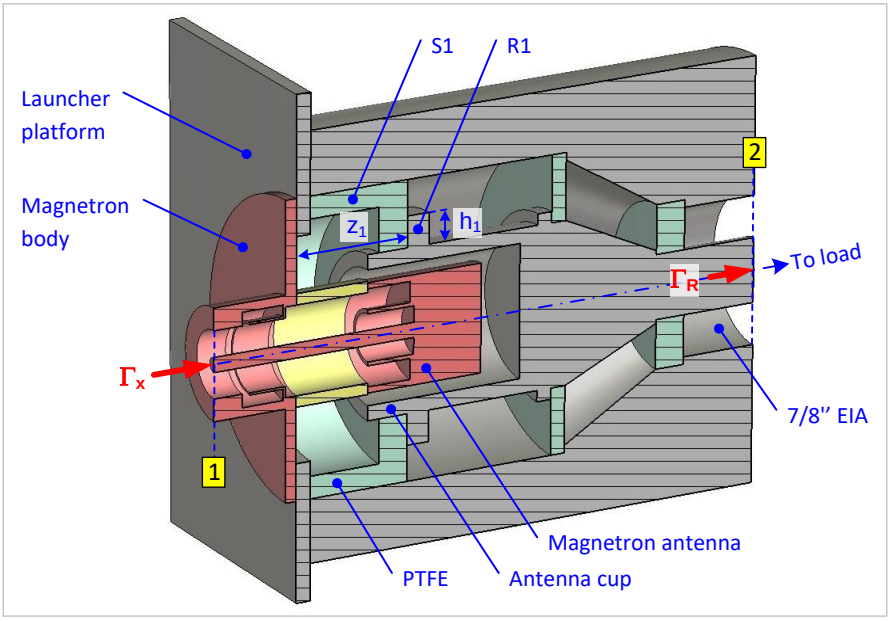

Fig. 3. CST model of the designed extended coaxial launcher (ECL).

When conceiving the basic CL structure, we strived to meet the following criteria:

1. The launcher should be as short as possible. We achieved an overall length for the designed launcher of 69 mm.
2. The coupling with the magnetron antenna should be noncontacting (capacitive), mainly to avoid the risk of sparking. Therefore, the inner CL conductor has the form of a cup enveloping the antenna. The cup must be sufficiently wide and deep to accommodate the slightly differing antenna dimensions of various magnetron models considered for use with the CL. After examining the effect of the radial gap, we chose its nominal width to be 2 mm.
3. The inner and outer conductors should provide a smooth yet not excessively long transition from the antenna cup to the output coaxial line. We accomplished this using a conical part that was about 13 mm long. Far from it being a truly smooth transition, the cone is long enough to avoid an excessive step discontinuity.
4. The inner conductor should be kept firmly in position. We accomplished this via a set of three PTFE spacers in combination with rims in the inner conductor and counterpart grooves in the outer body.
5. Variables should be available for comfortable adjustment (by simulation) of the launcher S_{11}. A typical impedance transformation method calls for the introduction of a controlled discontinuity at a defined distance from the input. We were able to implement this principle by changing the height h_1 and axial distance z_1 of the rim R1 as well as the dimensions of the input spacer S1.

We created an optimization task in CST Design Studio that seeks, by varying h_1 and z_1, to minimize the magnitude of the error vector e_{11} (4) in the frequency range 2.4 – 2.5 GHz. As the target $S_{R11}(f)$ function, we used the Touchstone file obtained previously for the ERL. The contours of the resulting S-parameters in 2.2 – 2.7 GHz band in comparison with those of the ERL are presented in Fig. 4a. The thicker curve portions correspond to the

optimization sub-band 2.4 – 2.5 GHz. The distance $|e_{11}|$ between $S_{11}(f)$ and $S_{R11}(f)$ is less than 0.025 in this sub-band, as evidenced by Fig. 4b. This is a small difference, promising a nearly identical magnetron performance in both launchers.

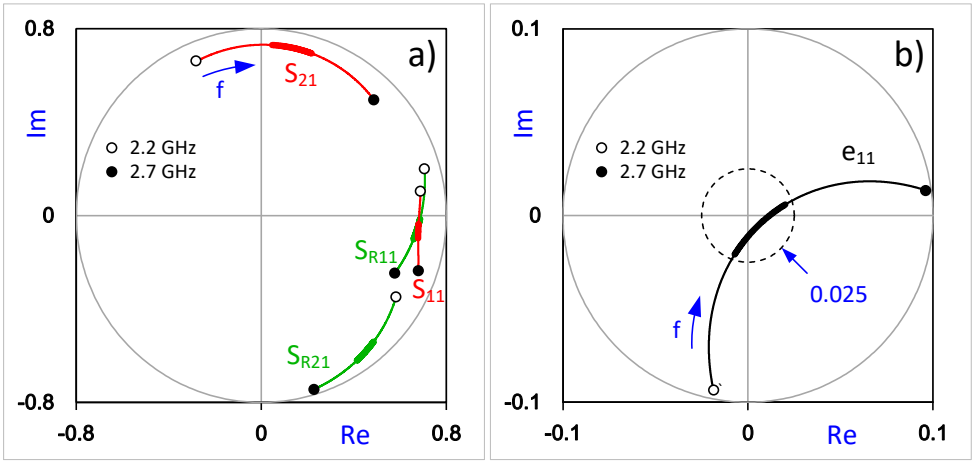

Fig. 4. a) S-parameters of the designed ECL (red) in comparison with ERL (green). b) Difference e_{11} between S_{11} (of ECL) and S_{R11} (of ERL). The thicker curve portions correspond to the optimization sub-band 2.4 – 2.5 GHz.

The *transmission* parameters S_{21} and S_{R21} are mutually phase-shifted (the shift is 132° at 2.45 GHz); also, the S_{21} contour is longer. This suggests that the ECL is electrically longer by a free-space distance of about 45 mm. It conforms with the differing position of the output reference plane 2, which is located at the antenna axis of the ERL but at a distance of 39 mm from the antenna tip of the ECL. Physically, however, the CL is significantly shorter than the datasheet-recommended RL (69 mm vs. 170 mm). The differing phases of S_{21} for the ERL and the ECL results in a mutual rotation between their Rieke diagrams.

The highest E-field strength in the whole ECL structure occurs within the interior of the magnetron, at the antenna wire close to the input plane 1. For an input power of 1.5 kW and a matched load, E_{max} = 726 V/mm. Outside of the antenna, (our main concern), E_{max} of merely 80 V/mm was detected at the edge of the antenna tip. This value is less than 3% of the air dielectric strength (3 kV/mm). In the ERL, the situation is very similar.

The highest surface current density ($J_{max} \approx 1.6$ A/mm) also occurred in the antenna wire, this time at its junction with the antenna cap. The estimated power loss in the wire is a negligible 1 W per 10 mm of the wire length. In the CL alone, the lost power is similarly small.

The results obtained for both E_{max} and J_{max} suggest that, with regard to arcing and overheating, the CL should not behave worse than the well-proven waveguide RL.

Rieke Diagram

For the purpose of experimental verification, we built a CL prototype (Fig. 5). As an ultimate criterion of the design success, we measured the Rieke diagram of a 2M244 magnetron installed in this CL. The experimental setup is shown in Fig. 6. The magnetron was water-cooled for better measurement repeatability. The measurement is based on a WR340 waveguide autotuner (S-TEAM STHT 1.4), which (a) automatically sets a sequence of tuning stub positions to approximately realize a predefined series of desired load reflection coefficients Γ_R; (b) for each setting, measures the *actual* Γ_R, the power P_L absorbed in the waterload, and the generated frequency f_g; and (c) writes the results to a text file, which will be further processed by a developed MATLAB procedure to create the

Rieke diagram. The load reflection coefficients Γ_R and, consequently, the obtained Rieke diagram, are referred to the plane of the launcher coaxial output (labelled 2 in Fig. 6). Full details of the measurement procedure are described in [5]. We used the same power supply and autotuner settings. Unlike [5], where Γ_R was moved along a rectangular grid, here Γ_R was stepped along circles of increasing radii. Thus, excessive jumps were avoided in P_L, and hence in the magnetron temperature, which had degraded the data consistency.

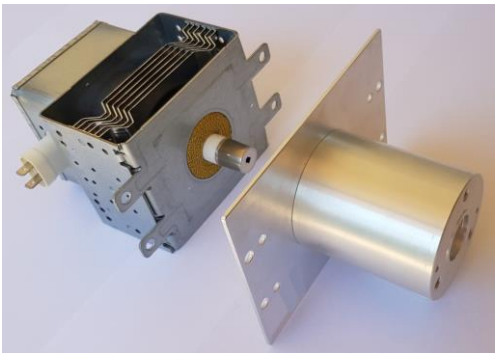

Fig. 5. Launcher prototype with a 2M244 magnetron ready to be installed.

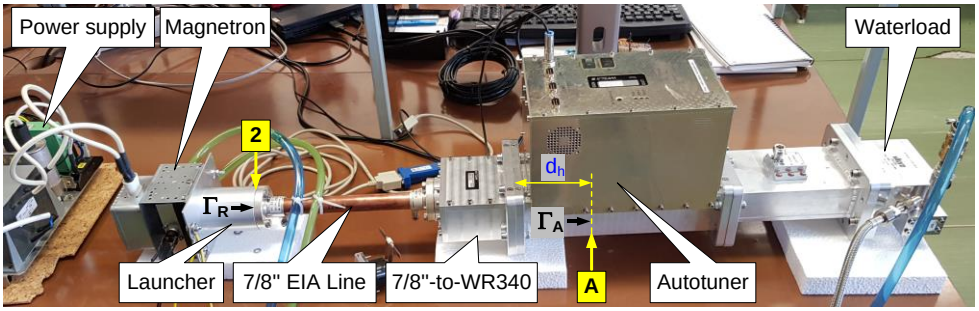

Fig. 6. Rieke diagram measurement setup.

The autotuner inherently measures the load reflection coefficient Γ_A, referred to a plane A located at the axis of the tuning stub closest to generator. Between the launcher under test and this plane is a cascade consisting of a 224.8 mm long section of 7/8" EIA transmission line, a coaxial-to-waveguide adapter (S-TEAM WTL171), and a section with length d_h = 132.3 mm of a WR340 waveguide internal to the autotuner. In order to compute Γ_R from Γ_A, the autotuner needs to know the scattering matrix of this network. We used theoretical values for the EIA line and the waveguide, and electromagnetic simulation of WTL171.

Fig. 7a shows the set of the desired Γ_R (661 points). The points are spaced equidistantly; the maximal Γ_R magnitude is 0.7. Fig. 7b shows the *actual* Γ_R measured in the process. Evidently, the data tend to be expelled from the unstable sink area of the magnetron, where the generated frequency is very sensitive to load variations.

Rieke diagrams obtained from the measured data are shown in Fig. 8a, b in the form of contours of constant frequency f_g and contours of constant power P_L. For comparison, we also measured the Rieke diagram of the same magnetron installed in a reference waveguide launcher (RL). The results are shown in Fig. 8c, d. It is evident that, apart from the expected overall rotation, the diagrams appear similar. A small visible difference is in the generated frequency f_{gm} for matched load $\Gamma_R = 0$. In the case of RL, f_{gm} = 2460 MHz, which is the specified 2M244 nominal frequency. In the case of CL, f_{gm} = 2462 MHz. This minor 2-MHz shift will have no practical consequences.

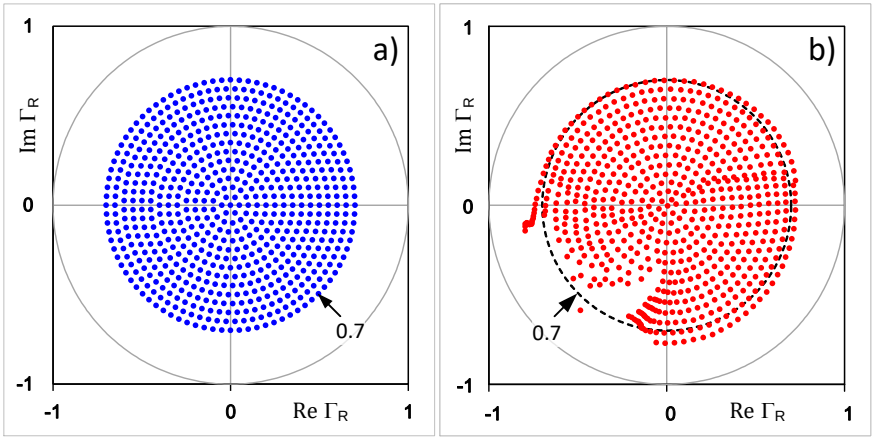

Fig. 7. Desired (a) and measured (b) set of load reflection coefficients Γ_R.

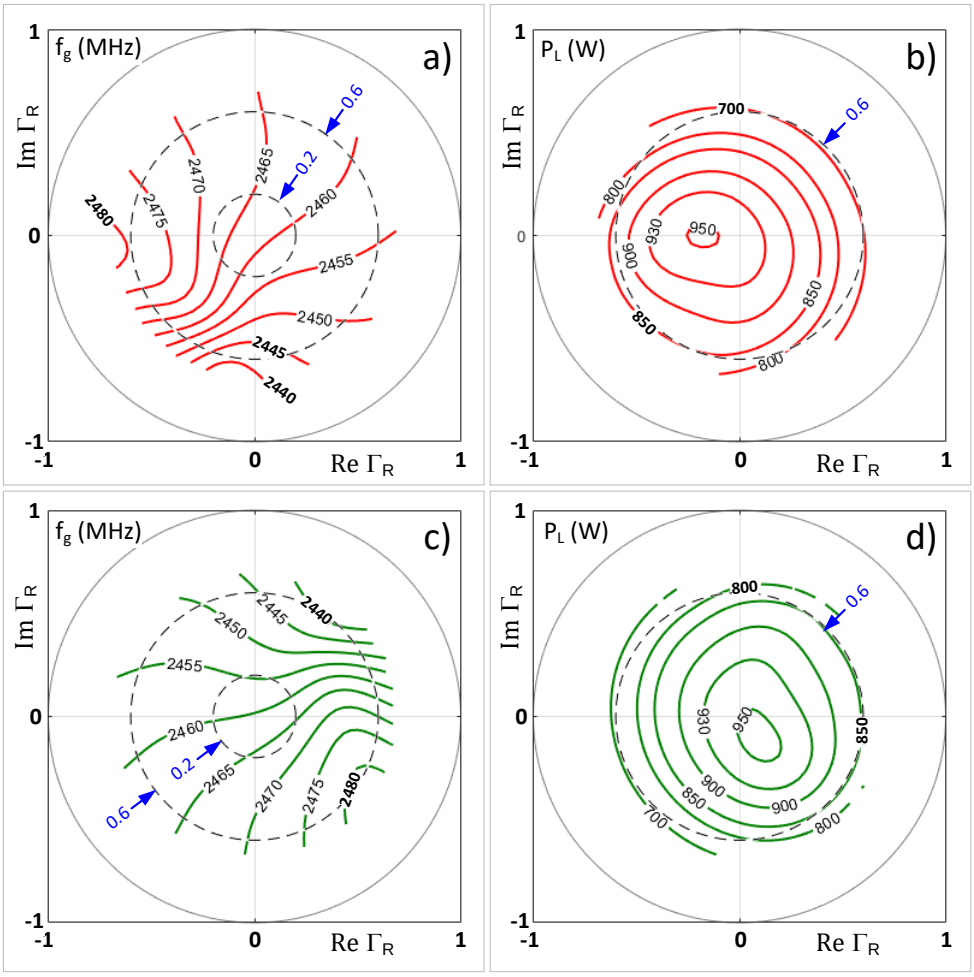

Fig. 8. Contours of (a) constant frequency and (b) constant power for a 2M244 magnetron installed in the designed coaxial launcher. (c, d) The same for the magnetron installed in a reference waveguide launcher.

The peak generated power is about 950 W in both cases. It is somewhat less than the 1010 W specified in the datasheet. The reason is that the power supply available for our experiments provided lower anode voltage than the specified 4.35 kV.

The circles with radius 0.2 are used for determining the frequency pulling figure Δf_p, which is defined as the maximal frequency difference observed when varying the phase of a load reflection coefficient with $|\Gamma_R| = 0.2$ (VSWR = 1.5). For both launchers, $\Delta f_p \approx 12$ MHz. The datasheet [3] specifies it nominally as 10 MHz, with a maximum of 15 MHz.

The circles with radius 0.6 represent the maximal permitted load reflection coefficient magnitude (VSWR = 4). In both launchers, the lowest generated power for this case is nearly the same (about 700 W). This means that in both launchers the power dissipated within the magnetron, and therefore the risk of its overheating, will also be the same.

Conclusions

We have developed a noncontacting coaxial magnetron launcher that is appropriate for a class of 2.45-GHz magnetrons with powers up to about 1.5 kW, with 7/8" EIA coaxial output. The design was focused on the Panasonic 2M244 magnetron, a good representative of this class. We completed the whole design using electromagnetic simulation. We verified the performance of the developed coaxial launcher by measuring the Rieke diagram of a 2M244 magnetron installed in a launcher prototype and in a standard waveguide reference launcher, stipulated by magnetron manufacturers. The comparison proved practically equal magnetron behavior in both launcher types. The developed coaxial launcher, thanks to its small dimensions and straightforward signal flow, will be beneficial in installations with coaxial inputs.

Acknowledgement

The author wishes to thank Dr. Shankar Rao for completing most of the Rieke diagram measurements, and for careful reviewing of the manuscript.

References

[1] Smith, G., Ed., *Microwave Magnetrons* (MIT RadLab Series, Vol. 6). New York: McGraw-Hill, 1948.
[2] Meredith, R. J., *Engineers' Handbook of Industrial Microwave Heating*. London: The IEE, 1998, DOI https://doi.org/10.1049/pbpo025e.
[3] Panasonic: *Continuous Wave Magnetron 2M244-M12*, Datasheet, Oct. 30, 2003.
[4] Dassault Systems: CST Studio Suite, https://www.3ds.com/products-services/simulia/products/cst-studio-suite/.
[5] Bilik, V, "Automatic Measurement of Magnetron Rieke Diagrams," in *Proc. AMPERE 2019: 17th Int. Conf. on Microwave and High Frequency Heating*, Valencia, 2019, pp. 478–486, DOI https://doi.org/10.4995/ampere2019.2019.9782.